Islamic Azad University

Journal of
Optoelectronical Nanostructures

Summer 2020 / Vol. 5, No. 3

Numerical Modeling of Electronic and Electrical Characteristics of $Al_{0.3}Ga_{0.7}N/GaN$ Multiple Quantum Well Solar Cells

Rajab Yahyazadeh[1], Zahra Hashempour[*,1]

[1] Department of Physics, Khoy branch, Islamic Azad University, Khoy, Iran

(Received 29 Jun. 2020; Revised 25 Jul. 2020; Accepted 18 Aug. 2020; Published 15 Sep. 2020)

Abstract: The present study was conducted to investigate current density of $Al_{0.3}Ga_{0.7}N/GaN$ multiple quantum well solar cell (MQWSC) under hydrostatic pressure. The effects of hydrostatic pressure were taken into account to measure parameters of $Al_{0.3}Ga_{0.7}N/GaN$ MQWSC, such as interband transition energy, electron-hole wave functions, absorption coefficient, and dielectric constant. Finite-difference method (FDM) was used to acquire energy eigenvalues and their corresponding eigenfunctions of $Al_{0.3}Ga_{0.7}N/GaN$ MQW and hole eigenstates were calculated through a 6×6 k.p method under an applied hydrostatic pressure. It was found that the depth of the quantum wells, bandgaps, band offset, the electron, and hole density increases with the hydrostatic pressure. Also, as the pressure increases, the electron and hole wave functions will have less overlap, the amplitude of the absorption coefficient increases, and the binding energy of the excitons decreases. Our results showed that a change in the pressure up to 10 GPa caused absorption coefficients̉ peaks of light and heavy holes to shift to low wavelengths of up to 32 nm, which in turn decreased short-circuit current density and increased open circuit voltage.

Keywords: Hydrostatic Pressure, Optical Absorption, Solar Cell, Multi-Quantum Well.

1. INTRODUCTION

Nitride heterostructures are important because of their high energy gap, high electron density in the quantum well, and high electrical conductivity [1,2]. These heterostructures are used in manufacturing of electronic components (e.g., transistors and diodes, optical components, and solar cells) and industrial components, such as electrical switches (disconnecting or connecting electrical circuits acting as converters) [3-5]. Binding energy of AlGaN/GaN excitons and

[*] Corresponding author. Email: Rajab.yahyazadeh@iaukoy.ac.ir

other optical behaviors may vary under the influence of external perturbations, such as temperature, magnetic field, and pressure [6,7]. Therefore, it is important to study the effect of hydrostatic pressure on optical and electrical parameters, such as electron and hole density, subband transition energy, current density, and absorption coefficient of $Al_{0.3}Ga_{0.7}N/GaN$ MQW. As the absorption coefficient is the most important parameter in calculating and studying current in solar cells, it needs to be studied under external pressure perturbation. Bardyszewski et al., studied binding energy of excitons under hydrostatic pressure [8]. Asgari et al., [9] calculated current density and absorption coefficient for InGaN / GaN MQWSC at different impurities and well widths. Petre et al., [10] calculated subband transition energy and absorption coefficient of AlGaAs / GaAs MQW. Most of the previous studies have presented analytical formula obtained from experimental results for absorption coefficient, which depends on energy gap used in calculation of photoelectric current of solar cells [10]. A precise measurement of current density in solar cells requires numerical calculations of absorption coefficient [11]. Therefore, in this paper, behavior of current density and absorption coefficient of $Al_{0.3}Ga_{0.7}N/GaN$ MQWSC was investigated under external pressure. The most important advantages of this numerical method and novelty of this work are the use of five important parameters: effective mass, energy gap, lattice constants, dielectric constant, quantum barrier, and well-thickness, which are simultaneously dependent on hydrostatic pressure and temperature. The effect of hydrostatic pressure on energy of heavy and light holes and transition energy of subbands was also considered. In this model, conduction band energy, wave functions, and energy subbands were measured from self-consistent solution of the Schrodinger and Poisson equation. Energy of hole valance bands (heavy and light hole), wave functions, and energy subbands were calculated using a 6×6 k.p method. In the calculations, up to 5 energy subbands were considered in quantum wells. The sample used in modeling was p–i–n solar cells with an AlGaN/GaN MQWSC structure within i-region. The p and n regions were based on GaN. Donor and acceptor concentrations in n- and p-region materials were assumed to be the same with $0.1\times10^{18} cm^{3}$, and 19 wells were considered in this work. Only the first subband transition (with uncoupled heavy and light hole states) was considered in this calculation. Current density and absorption spectrum of MQWSC structure were determined via these transition energies and wave functions. It should be notified that the calculated built-in polarization field for structures is about $\sim 10^{8} Vm^{-1}$. In this work, atmospheric and hydrostatic pressures were taken into account. That is, at zero hydrostatic pressure, only atmospheric pressure was applied. The results and discussions were obtained by calculating and drawing figures.

2. HETEROSTRUCTURE MODELING

2.1. Self-Consistent Solution of Schrödinger-Poisson Equations

MQW structure introduced for the model was constructed by an AlGaN with a bandgap energy of E_g^{AlGaN} for barriers and GaN in the wells, as schematically shown in Fig. 1. For obtaining accurate values for Fermi energy, energies of the quantized levels within 2DEG, potential profiles, wave function, and sheet carrier concentration for 2DEG in AlGaN/GaN heterostructures, both the Schrodinger and Poisson equations must be solved self-consistently. This was achieved by solving Schrodinger's equation and simultaneously taking into account electrostatic potential obtained from Poisson's equation, as well as image and exchange-correlation potentials using three-point finite-difference method (FDM) (see Appendix A). The Schrodinger and Poisson equations in quantum structures are introduced as follows: [13]:

$$-\frac{\hbar^2}{2}\frac{d}{dz}\left(\frac{1}{m_e^*}\frac{d\psi_n(z)}{dz}\right)+E_c(z)\psi_n(z)=E_n\psi_n(z) \tag{1}$$

$$\varepsilon_0\frac{d}{dz}\varepsilon_z(z)\frac{d}{dz}(V_H+V_P)=e^2\left[\frac{\sigma_b}{e}\delta(z-z_0)+N_D-n(z)\right] \tag{2}$$

Where, $\hbar$ represents the reduced Planck constant, m_e^* is the electron effective mass, E_c is the total potential function, ψ_n is the nth state wave function, with its associated nth state energy level E_n. In total potential $E_c(z)=V_B(z)+V_H(z)+V_{ex}(z)+V_P(z)$, $V_B(z)$ is the heterojunction band gap discontinuity; $V_H(z)$ is the effective Hartree potential, and $V_{ex}(z)$ is the exchange-correlation potential. $V_P(z)=eF_z z$ is the potential energy induced by polarization charges, and F_z is the electric fields in the well (F_w) and barrier (F_b) caused by spontaneous (SP) and piezoelectric(PZ) polarization (see Appendix B). In the Poisson equation, $\varepsilon_z(z)$ is the dielectric constant at the position z, z_0 is the interface of AlGaN and GaN position, N_D is the donor total density, $n(z)$ is the sheet concentration of the confined electrons, and σ_b is the polarization charges of interfacial density [14,15]. The current numerical model uses five parameters: effective mass, energy gap, lattice constants, dielectric constant, quantum barrier, and well-thickness, which are simultaneously dependent on hydrostatic pressure and temperature as following:

1- Basal strain is expressed from lattice of substrate a_s and epilayer $a_e(T,P,m)$:

$$\epsilon(T,P,m)=\left(a_c-a_e(T,P,m)\right)/a_e(T,P,m) \tag{3}$$

Lattice constants, as a function of temperature, alloy, and hydrostatic pressure are given as follows [17-20]:

$$a_e(T,P,m)=a_0(m)\left[\left(1+\beta\left(T-T_{ref}\right)\right)\left(1-P/3B_0\right)\right] \tag{4}$$

Where, $B_0=239GPa$ is the bulk modulus of sapphire. $\beta_{GaN}=5.56\times10^{-6}K^{-1}$ is the thermal expansion coefficient , $T_{ref}=300K^0$ and $a_0(m)=0.13989m+0.03862$ is the equilibrium lattice constant that is a function of composition [20, 21].

2- Here, $\varepsilon_{GaN}(T,P)$, $\varepsilon_{AlGaN}(m,T,P))$ are the dielectric constant of GaN, AlGaN, and $d_{Al_mGa_{1-m}N}(T,P)$ is the AlGaN barriers̓ thickness so that, they are given as follows [6,22 and 23]:

$$\varepsilon_{GaN}(T,P)=10\times\exp\left(10^{-4}(T-T_0)-6.7\times10^{-3}P\right) \tag{5}$$

$$\varepsilon_{AlGaN}(m,T,P)=\varepsilon^{GaN}(T,P)+0.03m \tag{6}$$

$$L_b=L_{Al_mGa_{1-m}N}(T,P)=L_{AlGaN}(0)\left[1-\left(S_{11}^{Al_mGa_{1-m}N}+2S_{12}^{Al_mGa_{1-m}N}\right)P\right] \tag{7}$$

$$L_w=L_{GaN}(T,P)=L_{GaN}(0)\left[1-\left(S_{11}^{GaN}+2S_{12}^{GaN}\right)P\right] \tag{8}$$

Here, $L_{AlGaN}(0)$ and $L_{GaN}(0)$ are the AlGaN and GaN layers̓ thickness without considering hydrostatic pressure and temperature. S_{11} and S_{12} are the elastic compliance constants [6, 23].

3- Band gap energy of AlGaN/GaN is as following [16,26]:

$$E_g(T,P)=E_g(0,0)+\gamma P+\sigma P^2+\left(\alpha T^2\right)/\left(T+T_e\right) \tag{9}$$

$E_g(0,0)$ stands for the band gap energy of GaN or AlGaN in the absence of hydrostatic pressure and at a temperature of 0 K. The suggested parameters used in Eq. (9) in our calculations were taken from a previous study (Ref 23).

4-In the Schrödinger's equation, electron effective mass m^* can be written as [24,25]:

$$\frac{m_0}{m_e^*\left(P,T,m\right)}=1+\frac{E_P^\Gamma\left(E_g^\Gamma\left(P,T,m\right)+2\Delta_{S0}/3\right)}{E_g^\Gamma\left(E_g^\Gamma\left(P,T,m\right)+\Delta_{S0}\right)} \tag{10}$$

Where, m_0 is the free electron mass, E_P^Γ is the energy linked to momentum matrix element, Δ_{S0} is the spin-orbit splitting ,and $E_g^\Gamma\left(P,T,m\right)$ is the band gap variation as a function of hydrostatic pressure and temperature. Effective masses of light hole (lh), heavy hole (hh), and spin-orbit split-off (so) are given by [26]:

$$\frac{m_0}{m_{lh}^*(P,T,m)}=(\gamma_1+2\gamma_2)+\frac{2E_p^\Gamma}{3E_g^\Gamma\left(P,T,m\right)} \tag{11}$$

$$\frac{m_0}{m_{hh}^*(P,T,m)}=(\gamma_1-2\gamma_2)+\frac{2E_p^\Gamma}{3E_g^\Gamma\left(P,T,m\right)} \tag{12}$$

$$\frac{m_0}{m_{so}^*(P,T,m)}=\gamma_1+\frac{2E_p^\Gamma}{3[E_g^\Gamma\left(P,T,m\right)+\Delta_{S0}]} \tag{13}$$

Where, γ_1 and γ_2 are the nonparabolicity parameters taken from Ref 24.

2.2. Hole Wave Functions and Energy Subbands

Hole wave functions and energy subbands were calculated along the Z axis using a 6×6 k.p method [27]. Hole distribution was calculated by summing contributions from 5 hole subbands. A formulation was used to calculate hole distribution as follows [29]:

$$P_{2D}\left(z\right)=\frac{m_h^*K_BT}{\pi\hbar^2}\sum_{i=1}^{5}\sum_{\upsilon}^{3}\left|g_i^\upsilon\left(z\right)\right|ln\left[1+\exp(\frac{E_i-E_F}{K_BT}\right] \tag{14}$$

Where, m_h^* is an average hole mass in the k_x-k_y plane, E_i represents the hole wave functions, $g_i^\upsilon\left(z\right)$ is the envelope function associated with n-th basis state of the Hamiltonian, summation over n is over the three basis states, and summation over j is over the hole wave functions. Envelope functions are normalized such that, $\sum_{\upsilon=1}^{3}\int_0^{L_{GaN}}\left|g_i^\upsilon\left(z\right)\right|^2dz=1$.

2.3. Absorption Spectrum

Optical absorption spectrum of multiple quantum well material in an electric field can be written as [11]:

$$\alpha(\hbar\omega,F)=M_{cv}^{2}(F).q_{ex}.L\left(\hbar\omega,E_{CV}^{1,1}(F)-E_{b}\right)+\int_{E_{CV}^{1,1}(F)}^{\infty}M_{cv}^{2}(F).Nq_{com}.K\left(E',E_{cv}^{1,1}(F)\right)L(\hbar\omega,E')dE' \quad (15)$$

Here , $L(\hbar\omega,E)=\Gamma_{hom}^{2}\Big/2\pi\left[(\hbar\omega-E)^{2}+\Gamma_{hom}^{2}\right]$ is the Lorentzian function where, $\hbar\omega$ is the photon energy, $E_{cv}^{1,1}(F)$ is the separation between n = l valence and conduction subbands, E_b is the exaction binding energy, Γ_{hom} is the full width at half maximum (FWHM) of homogeneous broadening caused by phonon interaction and tunneling through barriers, q_{ex}. and q_{com} are the oscillator strengths of excitonic and band -to -band transitions, respectively, N is the joint density of states between valence and conduction bands ,and K is the continuum shape of the Sommerfeld factor[11] . $M_{cv,P}=\int\psi_{c,P}^{*}(x)\psi_{v,P}(x)dx$ is the electron–hole overlap integral. It should be mentioned that the assumption of Elliot's theory regarding absorption used in this paper is: (i) a continuum of transitions between free particle states and (ii) excitonic transitions. Also, in excitonic transition, only the first exciton state, 1S is considered, and electric field (F) inside the generic jth layer (either QW or barrier) is given by electric displacements at interface (see Appendix B). Ratio of exciton area to level of continuum is giving by $q_{ex}/Nq_{com}=12R_y$ where, $R_y=(e^{4}\mu)\big/(8\varepsilon h^{2})$ is the Rydberg constant with μ as the reduced mass of exciton:

$$\mu=\frac{m_{\|c}^{*}.m_{\|v}^{*}}{m_{\|c}^{*}+m_{\|v}^{*}} \quad (16)$$

Where, e is the electron charge, permittivity of MQW material is assumed as an average of those for the well and barrier material, and $m_{\|c}^{*}$ and $m_{\|v}^{*}$ are the effective masses of electron and hole in plain of well. Masses of heavy and light holes differ from their values in perpendicular direction ($m_{\perp}^{*}$), which are given by [11]:

$$m_{\|hh}^{*}=\frac{4m_{\perp hh}^{*}.m_{\perp lh}^{*}}{3m_{\perp hh}^{*}+m_{\perp lh}^{*}} \quad (17)$$

$$m_{\|lh}^{*}=\frac{4m_{\perp hh}^{*}.m_{\perp lh}^{*}}{m_{\perp hh}^{*}+3m_{\perp lh}^{*}} \quad (18)$$

2.4. Current Density

The relationship between current density J and voltage V for a MQWSC is presented by [30]:

$$J(V) = J_{QW0}\left[1 + r_R\beta\right]\left[\exp\left(qV/k_BT\right) - 1\right] - J_{ph} \tag{19}$$

Where, J_{QW0} is the saturation current density, J_{ph} is the photocurrent density, k_B is the Boltzmann constant, q is the elementary charge, T is the temperature, r_R is the radiative enhancement rate ,and β is the ratio of current required to feed radiative recombination in intrinsic region at equilibrium to usual reverse drift current resulting from minority carrier extraction [30,31]. The term $r_R\beta$ accounts for radiative recombination within intrinsic region, which was developed by Anderson [30].Only radiative recombination was considered in this study [21]. Definition of the quantities involved in the above equation will be presented below. Saturation current density J_{QW0} is given by [32]:

$$J_{QW0} = \left(qD_n/L_n\right)n_{p0} + \left(qD_p/L_p\right)p_{n0} \tag{20}$$

Where, n_{p0} and p_{n0} are the thermal equilibrium electron and holes̉ concentration in n-type and p-type semiconductors, respectively. $D_n(T) = kT\mu_e(T)/e$ is the temperature dependence of carrier diffusion coefficients of electron, τ_n is the lifetime of electron. In this work, lifetime of carriers for AlGaN was equal to n = 6.5 ns [11]. L_n is the diffusion length for electron, which is expressed by: $L_n = \left(D_n \times \tau_n\right)^{0.5}$. $\mu_T(T)$ is the electron mobility. Its expression is available in the literature [30]. Radiative enhancement rate r_R represents the fractional increase in recombination in i-MQW region, as expressed by Anderson [31]:

$$r_R = 1 + f_W\left[\gamma_B\gamma_{DoS}^2 exp\left(\left(E_g^{AlGaN}(P,T) - E_g^{GaN}(P,T)\right)/k_BT\right)\right] \tag{21}$$

Where, $f_W = 0.5$ denotes to occupation in i-AlGaN MQW region, γ_B = 10 is the oscillator enhancement factor, and γ_{DoS} is the density-of-states enhancement factor. Ratio of current $\beta = \left(qWB_Bn_i^2\right)/\left(J_{QW0}\right)$ is related to i-MQW active region, with $W = N_W(L_W + L_b)$ is the width of i-MQW region. L_b is the width of a quantum barrier, L_W is the width of a QW ,and N_W is the number of QWs. $B_B = 1.5\times10^{-11} cm^3 s^{-1}$ [32] represents the recombination coefficient and $n_i = g_B \exp(E_B / nk_B T)$ is the intrinsic carrier density in i-MQW region. Where, $g_B = \left(2/h^3\right)\left(m_h m_e / m_0\right)^{3/4}\left(2\pi m_0 k_B T\right)^{3/2}$ and n are the ideality factor [34,35]. E_B represents the barrier height at AlGaN/GaN interface. Photocurrent density generated by incident photons is expressed by:

$$J_{ph} = q\phi_A\left(P,T,x\right) \tag{22}$$

Flux of photons absorbed by MQW-region is given by [36]:

$$\phi_A\left(P,T,x\right) = N_W \sum\nolimits_n N_{ph}\left(\lambda_n\right) exp\left[\alpha_w\left(\lambda_n,P,T,x\right)L_W\right]\Delta\lambda \tag{23}$$

Where, N_{ph} is a quantity associated with solar spectrum, λ_n is the photon wavelength, and $\Delta\lambda$ is the line width. Open circuit voltage is obtained by setting J as 0 [37]. Its expression is as follows:

$$V_{OC} = \left(k_b T/q\right)\left\{Ln\left(\left(J_{ph} + J_{QW0}\left(1+r_R\beta\right)\right)\Big/ J_{QW0}\left(1+r_R\beta\right)\right)\right\} \tag{24}$$

3. RESULTS AND DISCUSSION

In this paper, a numerical-analytical model was presented to calculate optical and electrical parameters of $Al_{0.3}Ga_{0.7}N/GaN$ MQWSC, under hydrostatic pressure. Iteration was conducted between the Schrödinger−Poisson equation systems by a three-point FDM to obtain a self-consistent solution of basic equations. During self-consistent calculation, a grid spacing as small as $1\times10^{-10} m$ was obtained and convergent criteria for electrostatic potential were set to be 0.1% to ensure iteration convergence and stability of our calculation. Hole eigenstates were calculated along the Z-axis using a 6×6 k.p method. Fig. 2 shows dependence of conduction band offset, bandgaps of AlGaN, and GaN to hydrostatic pressure. An increase in the hydrostatic pressure at a range of 0-10Pa led to the increase in the conduction band offset, which is attributed to an increase in the bandgap energy of GaN and AlGaN with an increase in the hydrostatic pressure. This phenomenon is related to correction of atomic distances in the crystal lattice by external pressure, also leading to a change in polarization. Fig. 2 also shows variations in the interface polarization charge density (σ_b) versus hydrostatic pressure. As the pressure increases, σ_b rises due to the increase in the piezoelectric polarization and spontaneity. With the increase in the hydrostatic pressure, lattice constants ($a_e\left(T,P,m\right), a_0\left(m\right)$) also increase.

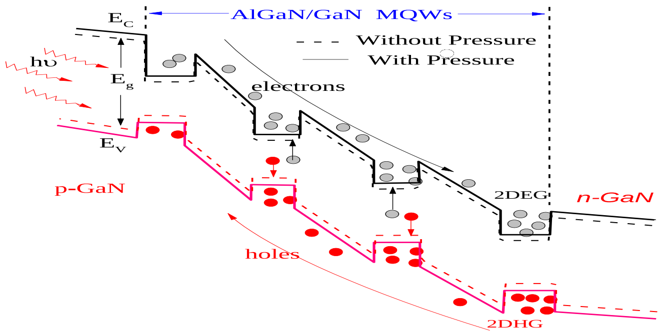

Fig. 1. Schematic profile of pGaN–i(AlGaN/GaN MQWSC)–n-GaN.

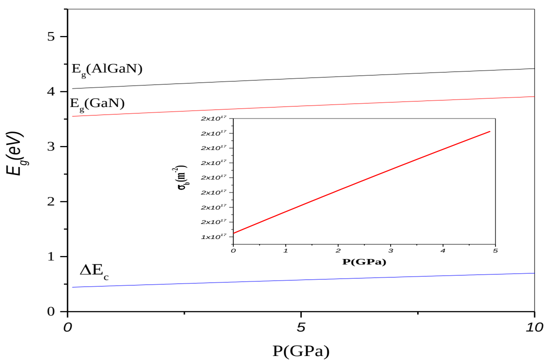

Fig. 2. The band-gaps energy of $Al_{0.3}Ga_{0.3}N$, GaN and conduction band offset of the $Al_{0.3}Ga_{0.3}N / GaN$ as a function of pressure and temperature. The insert indicates the variations in the σ_b versus pressure

Fig. 3 shows dependence of conduction and valance bands on hydrostatic pressure and location of quantum wells (electrons in the conduction band and holes in the valance band). With the increase in the pressure, energy gap also increases and the distance between subbands of quantum wells should also increase. Fig. 4 shows an example of a change in an electron quantum well to carefully study changes in the well and its subbands. Increasing hydrostatic pressure at the range of 0-10 GPa led to the increase in the quantum well depth to 75 meV, and subband energy was increased to 20 meV in absolute magnitude. Therefore, the first band was merely considered by wave functions and sub-energies to calculate transition energy $(E_{CV}^{1,1})$ and wave functions in overlap integral ($M_{CV}^{1,1}$) within the absorption relation.

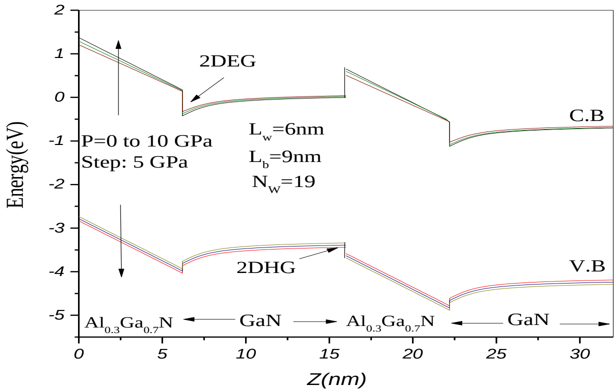

Fig. 3. The conduction(C.B) and valance(V.B) bands energy of $Al_{0.3}Ga_{0.7}N / GaN$ hetrostructure as a function of the distance under different hydrostatic pressure.

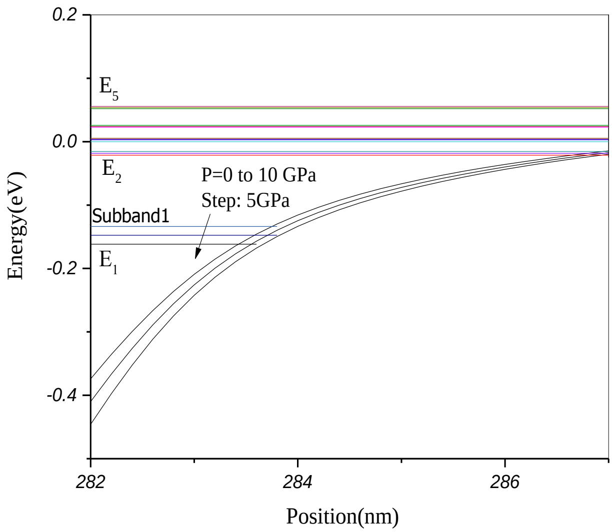

Fig. 4. The quantum well conduction band and subband of energy as a function of the distance under different hydrostatic pressure.

In this transition energy, the effect of light and heavy holes was also considered in the valance band.

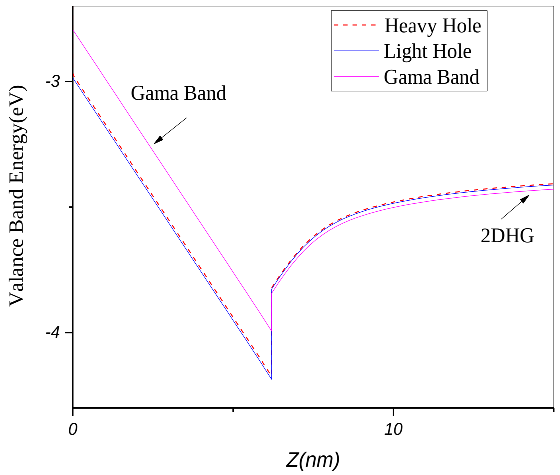

Fig. 5. Valance bands energy (Gama, light and heavy holes bands in the vicinity of 2DHG) versus distances for $Al_{0.3}Ga_{0.7}N / GaN$ hetrostructure.

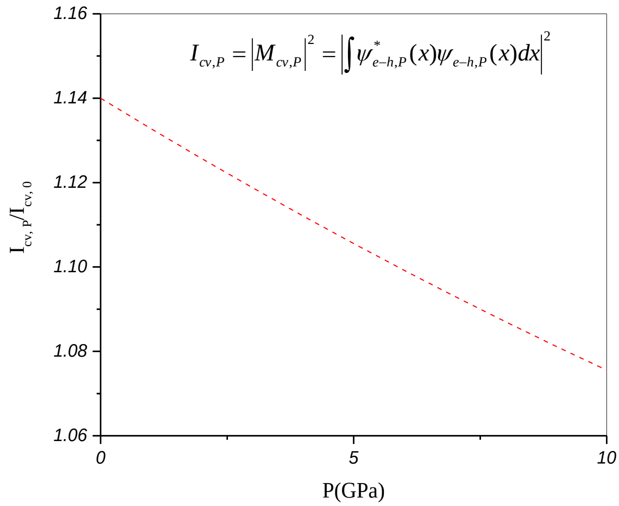

Fig. 6. Normalized square of the overlap of the electron–hole wave functions versus hydrostatic pressure.

Fig. 5 shows changes in the valance band energy (light and heavy holes in the vicinity of wells). Gamma band was not included in the calculations due to light and heavy holes. According to Fig. 5, energy difference between light and heavy holes was equal to 9 meV in the vicinity of hole well. This difference varied with pressure changes (similar to valance band changes in Fig. 3). Hole and electron overlap integral is another parameter that is important in calculating absorption coefficient. Fig. 6 shows dependence of the normalized square of overlap integral on hydrostatic pressure.

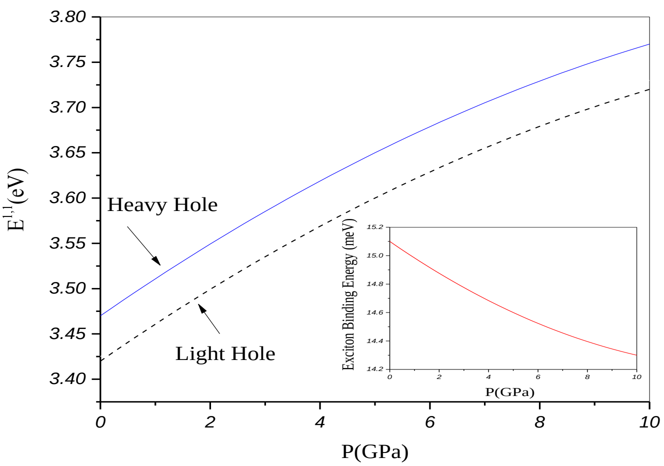

Fig. 7. The separation between the valance and conduction subbands ($E_{CV}^{1,1}$) versus hydrostatic pressure. The insert indicates the exciton binding energy versus pressure

As the pressure increases, separation between valance and conduction subbandș energy ($E_{CV}^{1,1}$) also increases as shown for light and heavy holes in Fig. 7. As a result, electron and hole wave functions will have less overlap. Low overlap indicates a decrease in the Coulomb energy of electron and hole. It means that exciton dependence energy decreases by increasing hydrostatic pressure as shown in the inset of Fig. 7. According to Fig. 8, after determining pressure dependence of wave functions, energy of subbands and overlap integral, absorption coefficient can be calculated from Eq. 11. Moreover, with the increase in the pressure, the absorbed photon energy also increases, as well as corresponding wavelength decreases, which are related to the increase in the bandgapș energy through pressure. In this figure, two peaks are observed for each pressure, which are associated with light and heavy holes of the valance band. According to Fig. 5, heavy holes have more energy and therefore, they will have a shorter wavelength than light holes, so small peaks are related to heavy holes. The second point is associated with changes in the amplitude of absorption coefficient. As the pressure increases, amplitude of absorption coefficient also increases.

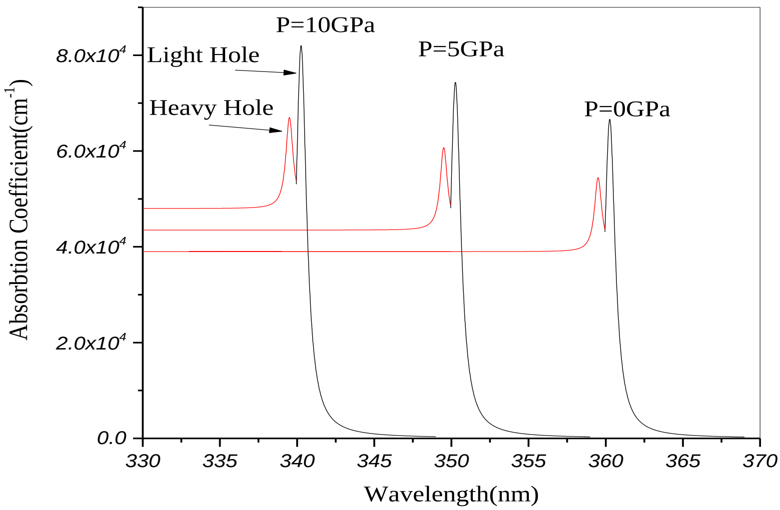

Fig. 8. Absorption coefficient for p-GaN–i($Al_{0.3}Ga_{0.7}N / GaN$ MQWSC)–n-GaN versus different hydrostatic pressure

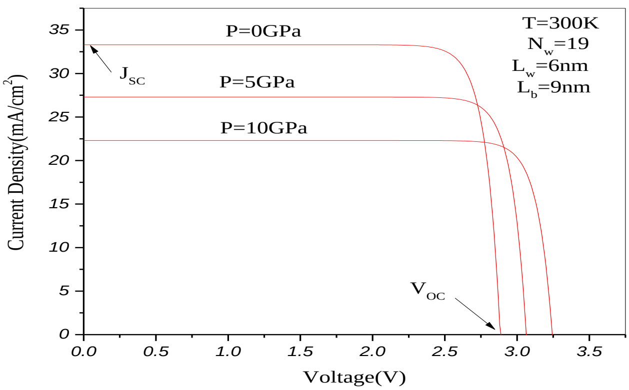

Fig. 9. Current-voltage characteristic of 20-MQW $Al_{0.3}Ga_{0.7}N / GaN$ solar cell for various hydrostatic pressure.

In other words, binding energy of the excitons decreases by increasing the pressure, and they will have a greater tendency to absorb energy and acquire a stronger binding. The stronger the binding energy, the lower the tendency to absorb energy. Therefore, increasing the pressure will enhance amplitude. Fig. 9 depicts curves of current-voltage for different hydrostatic pressure values. Hydrostatic pressure dependence of short-circuit current density (J_{SC}) and open circuit voltage (V_{OC}) for different pressure values can be seen in Fig. 12. In the case of P= 0GPa at room temperature, J_{SC} value was equal to $33.3 mAcm^{-2}$ and was further decreased to $22.2 mAcm^{-2}$ at P= 10GPa. However, short-circuit current density decreases by increasing hydrostatic pressure, due to the increase in the band gap energy. Furthermore, the increase in the band gap energy results in higher absorption of lower wavelength incident light, which will allow more wavelength electrons to jump into conduction band due to the presence of more free electrons leading to an increase in the current density. V_{OC} was increased almost linearly from 2.85 V at P= 0GPa to 3.32 V at P= 10GPa, which is mainly attributed to band-gap increment by increasing hydrostatic pressure.

4 CONCLUSIONS

In this study, optical absorption spectrum of $\mathrm{Al_{0.3}Ga_{0.7}N/GaN}$ MQWSC was investigated under hydrostatic pressure. The results showed that the increase in the pressure could enhance polarization charge density (σ_b). Increasing hydrostatic pressure at the range of 0-10GPa led to an increase in the conduction band discontinuity from 0.4 to 0.7eV and also an increase in the distance between the first subband of conduction band energy and capacity ($E_{CV}^{1,1}$) by 20meV. At each pressure, energy difference between light and heavy holes in the valance band was equal to 9meV. Increasing hydrostatic pressure at the range 0-10 GPa led to (I), an 8 mV decrease in the exciton bonding energy (corresponding to the first substrates), (II) an increase (height) in the absorption coefficient by 15.8 for heavy holes and 12.8 for light holes, (III) a decrease in the overlap of the normalized wave functions by 0.06, (IV) a decrease in the 32 nm of absorption coefficient peaks, as well as (V) a decrease in the short-circuit current density up to $10 mAcm^{-2}$ and an increase in the open circuit voltage up to 0.47V.

Appendix A: Numerical Method

Discretization of Schrodinger and Poisson equations was performed using FDM. A centered second -order scheme was used. Therefore, a continuous term, such as $\frac{d}{dz}\left(f\frac{d\psi}{dz}\right)$ is discretized as follows:

$$\frac{d}{dz}\left(f\frac{d\psi}{dz}\right)=\frac{\frac{(f_{i+1}+f_i)}{2}\times\frac{(\psi_{i+1}-\psi_i)}{\Delta z}}{\Delta z} \tag{A1}$$

The Schrodingers̓ equation is written as follows: $H\psi_i=E\psi_i$
Non-zero elements of matrix H are:

$$H(i,j)=\begin{cases}\dfrac{\hbar^2}{2m_0\Delta z^2}\dfrac{1}{2}\left(\dfrac{1}{m^*(i)}+\dfrac{1}{m^*(i-1)}\right) & if \quad j=i+1\\ \dfrac{\hbar^2}{2m_0\Delta z^2}\left(\dfrac{1}{2}\left(\dfrac{1}{m^*(i)}+\dfrac{1}{m^*(i-1)}\right)+\dfrac{1}{2}\left(\dfrac{1}{m^*(i)}+\dfrac{1}{m^*(i+1)}\right)\right)+E_c(i) & j=i\\ -\dfrac{\hbar^2}{2m_0\Delta z^2}\dfrac{1}{2}\left(\dfrac{1}{m^*(i)}+\dfrac{1}{m^*(i+1)}\right) & j=i+1\end{cases} \tag{A2}$$

It is straightforward to obtain matrix system related to the Poissons̓ equation. The above eigenvalues̓ system and linear system are coupled and should be solved using an iterative method. Convergence is obtained when the difference in the Fermi level associated with two consecutive iterations is smaller than $10^{-4}eV$. Boundary conditions related to the Schrodingers̓ equation are:

$$\psi_n(z=0)=\psi_n(z=L)=0 \tag{A3}$$

Where, L is the total height of the structure. Boundary conditions related to the Poissons̓ equation are:

$$\left.\frac{d(V_H+V_P)}{dz}\right|_{z=0}=\left.\frac{d(V_H+V_P)}{dz}\right|_{z=L}=0 \tag{A4}$$

Appendix B: Electric Fields

Assuming no free charge, electric displacements at interface between (j) th and $(j+1)$ th layers and between $(j+1)$ th and $(j+2)$ th layers can be expressed as follows:

$$\varepsilon_{j+1}\varepsilon_0 F_{j+1} = \varepsilon_j \varepsilon_0 F_j + P_j - P_{j+1} \tag{B1}$$

$$\varepsilon_{j+2}\varepsilon_0 F_{j+2} = \varepsilon_{j+1}\varepsilon_0 F_{j+1} + P_{j+1} - P_{j+2} \tag{B2}$$

Substituting from Eq.(B1) gives an expression for Eq.(B2):

$$\varepsilon_{j+2}\varepsilon_0 F_{j+2} = \varepsilon_j \varepsilon_0 F_j + P_j - P_{j+2} \tag{B3}$$

Where, ε_j represents the dielectric constants and P_j is the polarization in jth layer. It follows that the field in any layer is related to field in a particular layer as in the following:

$$F_k = \frac{1}{\varepsilon_k \varepsilon_0}\left(\varepsilon_j \varepsilon_0 F_j + P_j - P_k\right) \quad k = j+2 \tag{B4}$$

We focus on the case where there is no voltage difference across MQW either because thermodynamic equilibrium prevails or an applied field exists that compensates any built-in field. The condition, in which the volt value dropped across MQW is zero, is as follows:

$$\sum_k L_k F_k = L_j F_j + \sum_{k \neq j} L_k F_k \tag{B5}$$

Here, L_k and L_j are the kth and jth layers̓ thickness. Substituting from Eq.(B4) gives an expression for electric field in any layer:

$$F_j = \frac{\sum_{k \neq j}\left(P_k - P_j\right)\left(L_k / \varepsilon_k\right)}{\varepsilon_k \varepsilon_0 \sum_k \left(L_k / \varepsilon_k\right)} \tag{B6}$$

In the case of a MQW with only two types of layers (L_w and L_b), the fields are :

$$F_w = \frac{(P_b - P_w)L_b}{\varepsilon_0(\varepsilon_w L_w + \varepsilon_b L_b)} \quad , \; F_b = \frac{(P_w - P_b)L_w}{\varepsilon_0(\varepsilon_w L_w + \varepsilon_b L_b)} = -F_w \frac{L_w}{L_b} \qquad \text{(B7)}$$

In these equations, the difference in polarization density is equal to surface polarization density in AlGaN/GaN, which is calculated by the following equation:

$$\sigma_b = |P_b - P_w| = |P^{PZ}_{Al_mGa_{(1-m)}N} + P^{SP}_{Al_mGa_{(1-m)}N} - P_{GaN}{}^{SP} - P^{PZ}_{GaN}| \qquad \text{(B8)}$$

Where,

$$P^{PZ}_{GaN} = -0.918 \in +9.541 \in^2 \qquad \text{(B9)}$$

$$P^{PZ}_{GaN} = \begin{cases} -1.808 \in +5.624 \in^{(2)} \;\; for \in < 0 \\ -1.808 \in -7.888 \in^2 \;\; for \in > 0 \end{cases} \qquad \text{(B10)}$$

$$P^{SP}_{(Al_mGa_{(1-m)}\mathrm{N})} = 0.090m - 0.034(1-m) + 0.21x(1-m) \qquad \text{(B11)}$$

Here, $\in$ is the basal strain whose relation is equal to Eq. (3) presented in the main text.

REFERENCES

[1] R. Chu. *GaN power switches on the rise: Demonstrated benefits and unrealized potentials*. Appl. Phys. Lett. 116 (2020) 090502.

[2] G. Hu, L. Lib, Y. Zhang. *Two-dimensional electron gas in piezotronic devices*. Nano Energy. 59 (2019) 667–673.

[3] R. Yahyazadeh, Zahra hashempour, *Effects of Hydrostatic Pressure and Temperature on the AlGaN/GaN High Electron Mobility Transistors*. Journal of Interfaces, Thin films, and Low dimensional systems. 2(2) (2019) 183-194.

[4] R Yahyazadeh, Z. Hashempour. *Numerical Optimization for Source-Drain Channel Resistance of AlGaN/GaN HEMTS*. Journal of Science and technology. 11(1) (2019) 1-9.

[5] A. Horri, S. Z. Mirmoeini. Analysis of Kirk Effect in Nanoscale Quantum Well Heterojunction Bipolar Transistor Laser. Journal of Optoelectronical Nanostructures. 5(2) (2020) 25-38.

[6] C. M. Duque, A. L. Morales, M. E. Mora-Ramos, C. A. Duque. *Exciton-related 21optical properties in zinc-blende GaN/InGaN quantum wells under hydrostatic pressure*, Physica Status Solidi (b). 252 (2015) 670.

[7] Z.H. Zhang, J.H. Yuan, K.X. Guo. *The Combined Influence of Hydrostatic Pressure and Temperature on Nonlinear Optical Properties of* $Al_{0.3}Ga_{0.7}As/GaAs$ *Morse Quantum Well in the Presence of an Applied Magnetic Field*. Materials, 11 (2018) 668.

[8] W. Bardyszewski, S.P. Lepkowski, H. Teisseyre, *Pressure Dependence of Exciton Binding Energy in GaN/AlxGa1-xN Quantum Wells*. Acta Physica Polonica A, 119(5) (2011) 663.

[9] A.Asgari , Kh.Khalili. *Temperature dependence of InGaN/GaN multiple quantum well based high efficiency solar cell*. Solar Energy Materials& SolarCells, 95 (2011) 3124.

[10] M. Cheraghizade. *Optoelectronic Properties of PbS Films: Effect of Carrier Gas*. Journal of Optoelectronical Nanostructures. 4(2) (2019) 1-12.

[11] P. J. Stevens, M. Whitehea, G. Parry, K. Woobridge. *Computer Modeling of the Electric Field Dependent Absorption Spectrum of Multiple Quantum Well Material*. IEEE Journal of Quantum Electronics. 24 (1988) 2007.

[12] Bi. Chouchen, M. H. Gazzah, A. Bajahzar, Hafedh Belmabrouk, *Numerical Modeling of the Electronic and Electrical Characteristics of InGaN/GaN-MQW Solar Cells*, Materials. 12 (2019) 1241.

[13] R. Belghouthi, J. P. Salvestrini, M. H. Gazzeh, and C. Chevallier. *Analytical modeling of polarization effects in InGaN double hetero-junction p-i-n solar cells*, Superlattices and Microstructures. 100 (2016) 168.

[14] Bi. Chouchen et al., *Numerical modeling of InGaN/GaN p-i-n solar cells under temperature and hydrostatic pressure effects*, AIP Advances 9 (2019) 045313.

[15] X. Huang, Piezo-Phototronic Effect in a Quantum Well Structure. ACS Nano, 10(5) (2016) 5145.

[16] O. Ambacher, A. B Foutz, J Smart, J. R Shealy, N. G Weimann, K Chu, et al. *Two dimensional electron gases induced by spontaneous and piezoelectric polarization in undoped and doped AlGaN/GaN heterostructures*. J. Appl. Phys, 87 (2000) 334.

[17] S. Z. H. Minabi, A. Keshavarz, A. Gharaati. The effect of temperature on optical absorption cross section of bimetallic core-shell nano particles. Journal of Optoelectronical Nanostructures.1(3) (2016) 62-75.

[18] O. Ambacher, J. Majewski, C. Miskys, et al. *Pyroelectric properties of Al (In) GaN/GaN hetero- and quantum well structures*. J. Phys. Condens. Matter, 14 (2002) 3399.

[19] Z. J. Feng, Z. J. Cheng, and H. Yue, *Temperature dependence of Hall electron density of GaN-based heterostructures*. Chinese Physics. 13 (2004) 1334.

[20] V. Fiorentini, F. Bernardini, and O. Ambacher, *Evidence for nonlinear macroscopic polarization in III–V nitride alloy Heterostructures*, Appl. Phys. Lett, 80 (2002) 1204.

[21] P. Perlin, L. Mattos, N. A. Shapiro, J. Kruger, W. S. Wong, T. Sands, N. W. Cheung, and E. R. Weber. *Reduction of the energy gap pressure coefficient of GaN due to the constraining presence of the sapphire substrate*. J. Appl. Phys. 85 (1999) 2385.

[22] K.J Bala, A. J Peter, and C. W Lee. *Simultaneous effects of pressure and temperature on the optical transition energies in a Ga0.7In0.3N/GaN quantum ring*. Chemical Physics. 495 (2017) 42.

[23] M. Yang et al., *Effect of polarization coulomb field scattering on parasitic source access resistance and extrinsic transconductance in AlGaN/GaN heterostructure FETs*, IEEE Trans. Electron Devices, 63 (2016) 1471.

[24] I. Vurgaftman, J. R Meyer, L. R. R Mohan, *Band parameters for III–V compound semiconductors and their alloys*. J. Appl. Phys, 89 (2001) 5815.

[25] S. Z. H. Minabi, A. Keshavarz, A. Gharaati. *The effect of temperature on optical absorption cross section of bimetallic core-shell nano particles.* Journal of Optoelectronical Nanostructures.1(3) (2016) 62-75.

[26] K.H. Yoo, L.R.Ram-Mohan, D.F.Nelson, *Effect of nanparabolicity in* $Al_xGa_{1-x}N/GaAs$ *semiconductor quantum well*. Phys. Rev. B. 39 (2089) 809.

[27] P. Perlin, L. Mattos, N. A. Shapiro, J. Kruger, W. S. Wong, T. Sands, N. W. Cheung, E. R. Weber. *Reduction of the energy gap pressure coefficient of GaN due to the constraining presence of the sapphire substrate.* J. Appl. Phys, 85 (1999) 2385.

[28] B. Jogai, *Influence of surface states on the two-dimensional electron gas in AlGaN/GaN heterojunction field-effect transistors*. Journal of Applied Physics, 93 (2003) 1631.

[29] B. Jogai, *Parasitic Hole Channels in AlGaN/GaN Heterojunction Structures*, phys. stat. sol. (b). 233(3) (2002) 506.

[30] B. Chouchen et al. *Numerical Modeling of the Electronic and Electrical Characteristics of InGaN/GaN-MQW Solar Cells*. Materials. 12 (2019) 1241.

[31] N.G. Anderson, *Ideal theory of quantum well solar cells*, J. Appl. Phys, 78 (1995) 1850.

[32] Y. Zhang, Y. Yang, Z.L. Wang. *Piezo-phototronics effect on nano/microwire solar cells*. Energy Environ. Sci, 5 (2012) 6850.

[33] Z. Podlipskas et al. *The detrimental effect of AlGaN barrier quality on carrier dynamics in AlGaN/GaN interface*. Scientific Reports. 9 (2019) 17346.

[34] *Handbook of Nitride Semiconductors and Devices: GaN-Based Optical and Electronic Devises*, 3rd ed., Wiley-VCH Verlag GmbH & Co. KGaA, Weinheim, Germany, 2009, 767-810.

[35] J. Nelson, *Thin Film solar cell*, *The Physics of Solar Cells*, *5*th ed. Imperial College Press, London, UK: WC2H 9HC, 2003, 211-251.

[36] Q. Deng et al., *An investigation on InxGa1-xN/GaN multiple quantum well solar cells*, J. Phys. D Appl. Phys. 44 (2011) 265103.

[37] Y. Sefidgar, H. R. Saghai, H. G. K. Azar. *Enhancing Efficiency of Two-bond Solar Cells Based on GaAs/InGaP.* Journal of Optoelectronical Nanostructures.4(2) (2019) 84-102.